A Self-healing Hydrogel Electrolyte Towards All-in-one Flexible Supercapacitors

Wen-Bin Ma
China University of Mining and Technology
Ke-Hu Zhu
China University of Mining and Technology
Shi-Fang Ye
China University of Mining and Technology
Yao Wang
China University of Mining and Technology
Lin Guo
China University of Mining and Technology
Xue-Yu Tao (taoxueyu@cumt.edu.cn)
China University of Mining and Technology https://orcid.org/0000-0003-2413-3740
Li-Tong Guo
China University of Mining and Technology
He-Liang Fan
China University of Mining and Technology
Zhang-Sheng Liu
China University of Mining and Technology
Ya-Bo Zhu
China University of Mining and Technology
Xian-Yong Wei
China University of Mining and Technology

Original Research

Keywords: Self-healing, Hydrogel electrolyte, All-in-one, Supercapacitor

Posted Date: February 9th, 2021

DOI: https://doi.org/10.21203/rs.3.rs-175256/v1

Version of Record: A version of this preprint was published at Journal of Materials Science: Materials in Electronics on July 22nd, 2021. See the published version at https://doi.org/10.1007/s10854-021-06555-5.

A self-healing hydrogel electrolyte towards all-in-one flexible supercapacitors

Wen-Bin Ma[1], Ke-Hu Zhu[1], Shi-Fang Ye[1], Yao Wang[1], Lin Guo[1], Xue-Yu Tao[1*], Li-Tong Guo[1], He-Liang Fan[1], Zhang-Sheng Liu[1], Ya-Bo Zhu[1], Xian-Yong Wei[2,3]

Abstract

The autonomously self-healable all-in-one supercapacitor is prepared by *in situ* rapid polymerization of electrode materials on the surface of self-healing poly (vinyl alcohol) (PVA) hydrogel electrolyte containing sulphuric acid (H_2SO_4). The self-healing PVA electrolyte has been achieved by physical interaction, in which dynamic hydrogen bonds between PVA chains can readily break and reform, allowing PVA hydrogel electrolyte to self-heal and regain its mechanical and electrochemical properties. The obtained PVA hydrogel displays fast self-healing capability, reliable mechanical performance (stress at 290 KPa after stretching to 238 %) and high ionic conductivity (57.8 mS cm^{-1}). Based on these excellent properties, an all-in-one supercapacitor with self-healing characteristics is assembled by in situ polymerization of aniline on the surface of self-healable PVA

* Corresponding author.

Email address: taoxueyu@cumt.edu.cn.

[1] *School of Materials Science and Engineering, China University of Mining and Technology, Xuzhou 221116, Jiangsu, China*

[2] *School of Chemical Engineering and Technology, China University of Mining and Technology, Xuzhou 221116, Jiangsu, China*

[3] *Key Laboratory of Coal Processing and Efficient Utilization, Ministry of Education, China University of Mining and Technology, Xuzhou, 221116, Jiangsu, China*

electrolyte. The self-healable all-in-one supercapacitor exhibits specific capacitance 470 mF cm^{-2} at current density of 0.2 mA cm^{-2} and energy density 32 μWh cm^{-2} at power density 100 μW cm^{-2}. The broken device can be repaired itself and there is a 63% capacitance retention for the healable supercapacitor. This self-healing supercapacitor will promote the development of self-healing energy storage devices in wearable electronics.

Keywords: Self-healing; Hydrogel electrolyte; All-in-one; Supercapacitor

1. Introduction

Flexible electronic devices have received broaden attention due to the booming market of wearable and portable products. This kind of equipment are often applied under various mechanical loads such as stretch, bend and are easily broken. It is a feasible solution to strengthen the flexible electronic devices and give them self-healing performance. On the one hand, the flexible self-healing electronic devices, including self-healing transistors [1, 2], sensors [3-5], electronic skin [6, 7], supercapacitors [8-10] and so on, are still competent in wearable and portable products. On the other hand, self-healing characteristics can extend these devices' service life under mechanical load by spontaneously healing its wound surface after being damaged, thus healing their mechanical and electrochemical properties. These advantages will greatly affect the existing energy storage devices, which are essential in several modern electronics.

Among various flexible energy storage devices, supercapacitors have been made great progress because of their fast charging and discharging process, high power density and

good cycle life [11]. In self-healing supercapacitors, the self-healing polymers serve as substrates, coating shells or electrolytes is the basis of healable mechanical integrity, while the healing of conductivity is based on the recovery of mechanical integrity [12]. According to previous reports, Jingquan Han et al. [13] synthesized self-healing polyaniline-cellulose nanofiber electrode by combining self-healing PVA hydrogel with capacitive polymer active material. This work actually sacrifices the mass and volume of the electrode in exchange for the ability of self-healing. And Minfeng Chen et al. [14] prepared the borax-crosslinked polyvinyl alcohol/nanocellulose hydrogel electrolyte, and assembled supercapacitor by clamping non-self-healing activated carbon paper electrode on the electrolyte. . Although this method does not sacrifice the performance of active components, the components with self-healing performance are independent from other components, which is not conducive to the overall self-healing of devices. Based on this method and the research of Wang et al. [15], Ying Guo et al. [16] initially constructed an integrated self-healing supercapacitor, avoiding the defects of delamination and high interface resistance in the laminated design. However, no further research has been done on the self-healing performance of the device, and the capacitance performance is not satisfactory in their research.

As mentioned above, self-healing polymers play a crucial role in self-healing supercapacitors. Among the various self-healing materials [17-21], Poly (vinyl alcohol) (PVA) has been studied intensively for the good gel forming and physical properties, high hydrophilicity, processability and biocompatibility [22, 23]. As has been reported, PVA

hydrogel can be prepared by chemically crosslinked by some crosslinkers, physically crosslinked by microcrystalline region and irradiation [22, 24]. To obtain the self-healing hydrogel, physical crosslinking is a facile method by freezing and thawing cycles. If it is not treated under low temperature cycles, the gel will be too viscid to remove from mold and not stable in water solution, so it is often used in the laminated supercapacitor. On the contrary, the gel will be a membrane with good mechanical property compatible with the all-in-one configuration supercapacitor. And the degree of crosslinking and the mechanical performance of PVA hydrogel are affected by cycles of freezing-thawing treatment [25]. Gupta, Siddhi et al. [26] prepared a PVA hydrogel through 45 freezing-thawing cycles and it possessed the stiffness of 33.25 MPa. Navid Samadi et al. [27] prepared a triple networks hydrogel based on Agar/PVA/Graphene, and it demonstrated autonomous self-healing within a short time of 10 min. Hui Peng et al. [28] has prepared a B-PVA/KCl/GO hydrogel electrolyte and endowed the active carbon based supercapacitor self-healing property without external stimulus. Therefore, PVA hydrogel electrolyte prepared by freezing and thawing cycles is employed as the self-healing substrate and electrolyte for the all-in-one configuration supercapacitor.

To construct a supercapacitor system, electrode materials play another important role. The capacitive materials for electrode application include carbon materials [29-31], metallic oxide [32, 33], conductive polymer [34, 35], and their composite. As one of the most widely studied conductive polymer electrode materials, polyaniline (PANI) shows the advantages of good thermal stability, biocompatibility [13], excellent capacitive

property and cyclic stability. For example, J. P. Pouget et al. [36] have investigated the structure of PANI by XRD and discussed the relationship of crystallite size, protonation and the conductivity of PANI. Yingxi Lin et al. [37] grew the nano-wire PANI electrodes on the surface of carbon cloth by electrodeposition, and the two electrodes were sandwiched to a PAA hydrogel electrolyte to obtain a supercapacitor. This device exhibited a specific capacitance of 217.43 F g^{-1}. Our group has also investigated the structure, electrochemical properties of PANI and its application on gel electrodes [38-40]. In addition, PANI can be easily integrated on the surface of hydrogel electrolyte by in-situ chemical oxidation polymerization to form an all-in-one device. Thus, PANI electrode material has been employed for the research of all-in-one self-healing supercapacitor.

Herein, a robust and self-healing PVA hydrogel electrolyte is prepared by physically crosslinking. After several low temperature treatments, the hydrogen bonds are gradually formed between the hydroxyl groups on PVA chains. Then the hydrogel is endowed with self-healing property. The obtained hydrogel possesses good mechanical properties (the stress strength at 238% tensile strain is 0.29 MPa) and ionic conductivity (57.8 mS cm^{-1}). Its self-healing performance is also researched (after 10th healing, its ionic conductivity is still 25.9 mS cm^{-1}). Based on the flexible self-healing hydrogel electrolyte, an all-in-one self-healing supercapacitor is assembled by in situ growing the polyaniline on the gel surface. After changing the aniline concentration, the supercapacitor displays an outstanding electrochemical performance of 470 mF cm^{-2} at current density of 0.2 mA

cm^{-2} and a large energy density of 32 μWh cm^{-2} while the power density is 100 μW cm^{-2}. Moreover, the broken device can be healed by itself with a capacitance retention rate of 63%.

2. Experiment

2.1 Materials

Polyvinyl alcohol (PVA, average molecular weight 74800-79200 g mol^{-1}), aniline and ammonium persulfate (APS) were obtained from Sinopharm Chemical Reagent Co., Ltd. Shanghai, China. All other reagents used in this research were analytically pure and used without further purification. All reagents used in this study were analytically pure, and no further purification was needed.

2.2 Preparation of self-healing PVA/H_2SO_4 hydrogel electrolyte membrane

The physical crosslinking PVA hydrogel was prepared by freezing-thawing cycles method. In a typical process, 2.6 g of polyvinyl alcohol powder was added to 15 ml of aqueous solution containing sulfuric acid with different concentrations. The mixture was heated at 90 ℃ in a water bath with violent stirring until the solution was clear. The solution was ultrasonically vibrated to remove bubbles, and then poured into a Petri dish. After the liquid level was flat, the petri dish was placed in a refrigerator at -20 ℃. After 3 h, the Petri dish was placed at room temperature to thaw the gel. Three freezing-thawing cycles were carried out to obtain the self-healing PVA/H_2SO_4 hydrogel electrolyte membrane. The concentration of the H_2SO_4 was changed as 0.01, 0.5, 1, 2, and 3 mol L^{-1}.

2.3 Preparation of self-healing PVA/H_2SO_4-PANI hydrogel membrane

The PVA/H_2SO_4-PANI hydrogel membrane was prepared by in situ chemical oxidative polymerization process. Firstly, aniline and APS were dissolved in 50 mL 1M H_2SO_4 solution to obtain solution A and solution B, respectively. And the molar ratio of aniline and APS was kept constant 1:1. Secondly, a piece of PVA/H_2SO_4 gel electrolyte membrane was immersed in solution A under magnetic stirring for 30 min. Then, solution B was dropped into the mixture of hydrogel membrane and solution A to initiate polymerization of aniline. The reaction was carried out with magnetic stirring at 0-5 ℃ for 3 h. Finally, the hydrogel membrane was taken out, and by-products on the surface of PANI layer were washed with deionized water and alcohol. The self-healing PVA/H_2SO_4-PANI hydrogel membrane was obtained, and the concentration of aniline was changed as 0.05, 0.1, 0.2, 0.3 and 0.4 mol L^{-1}.

2.4 Material characterizations

The PVA/H_2SO_4 hydrogel membranes and PVA/H_2SO_4-PANI hydrogel membranes were frozen in a refrigerator at -20 ℃ for 12 h and freeze-dried in a freeze dryer at -60 ℃ for 24 h to obtain lyophilized gel samples (PVA/H_2SO_4 hydrogel membranes and PVA/H_2SO_4-PANI hydrogel membranes). The morphology of lyophilized gel samples was characterized by scanning electron microscopy (SEM, SU8220, Hitachi, Japan). And the lyophilized gel samples were subjected to X-ray diffraction (XRD) using a Bruker D8 ADVANCE diffractometer equipped with Cu Kα radiation (λ=1.5418 Å). The infrared absorption spectrum of lyophilized gel samples was obtained by attenuated total

reflection Fourier transform infrared spectrometer (ATR-FTIR, Nicolet iS5, Thermo Fisher, America) at room temperature.

2.5 Tensile experiments

The mechanical tensile properties of the PVA/H_2SO_4 hydrogels were studied by the Electron Universal Testing Machines (MC009-WDW-20). The hydrogel membranes were cut into strips with dimensions of 80 mm × 20 mm × 2 mm. Tensile measurement was carried out by uniaxially stretching the hydrogel strips at a rate of 50 mm min^{-1}.

2.6 Fabrication and electrochemical measurements of the all-in-one self-healing supercapacitors

The PVA/H_2SO_4-PANI hydrogel membrane was cut off the edge connection to form a supercapacitor with a size of 30 mm × 10 mm × 2 mm. Then carbon cloth strips were used as current collection and would connect the supercapacitor and the electrochemical workstation system (CHI660 E, Shanghai ChenHua Co., Ltd, China).

Cyclic voltammetry (CV) scans was from -0.2 to 0.8 V at various scan rates of 5, 10, 20, 50 and 100 mV s^{-1}. Galvanostatic charge/discharge (GCD) was carried out at current densities of 0.2, 0.5, 1, 2 and 3 mA cm^{-2}, and the voltage ranges from -0.2 to 0.8 V. Electrochemical impedance spectroscopy (EIS) was taken at open circuit potential over the frequency range from 100,000 Hz to 0.01 Hz with a potential amplitude of 5 mV. All electrochemical experiments were carried out at room temperature.

The specific areal capacitance (C_A) of the supercapacitors based on single PANI electrode calculated from GCD curves is respectively derived from the equations:

$$C_A = \frac{2 \times I \times t}{A \times V} \quad (1)$$

where I, t, A, and V are the discharge current, discharge time from GCD curves, electrode area and potential window respectively.

The Energy density (E_A) and Power density (P_A) of the supercapacitors are obtained based on equations (2) and (3), respectively:

$$E_A = \frac{1}{2} \times C_A \times V^2 \quad (2)$$

$$P_A = \frac{E_A}{t} \quad (3)$$

The ionic conductivity (σ) of the PVA/H_2SO_4 hydrogel electrolyte is examined by the equation:

$$\sigma = \frac{d}{R \cdot S} \quad (4)$$

where d and S are the thickness and area of the PVA/H_2SO_4 hydrogel electrolyte sample, respectively. R is the bulk resistance obtained from EIS, which is the intercept on the real impedance axis in high frequency area of the Nyquist plot.

2.7 Self-healing test

A hydrogel electrolyte or an all-in-one supercapacitor were cut off and then the fracture surfaces were contacted for 20 min to repair themselves. The ionic conductivity of healed electrolyte was tested and then compared with the initial value to study its self-healing performance. And the CV, GCD and EIS were used to test the healed supercapacitor to investigate whether its electrochemical performance was repaired.

3. Results and discussion

Figure 1

The self-healing PVA/H_2SO_4 hydrogel electrolyte was facilely synthesized by physical crosslinking with hydrogen bonds. The preparation process is shown in Fig. 1. PVA powder was dissolved in H_2SO_4 aqueous solution under vigorous stirring until the blend solution became clear. Then the hydrogel was formed after three freezing-thawing cycles, which is shown in Fig. 1 a-d. For a freeing-thawing cycle, the blend is frozen at -20 ℃ for 3 h and then thawed at room temperature for 1 h. During the freezing-thawing cycles, as shown in Fig. 1e, hydrogen bonds were formed gradually between a large number of hydroxyl groups (-OH) on PVA. As shown in fig. 1e, during the freeze-thaw cycle, a large number of hydroxyl groups (-OH) on polyvinyl alcohol gradually form hydrogen bonds. PVA chains are cross-linked to form 3D networks held by the physical cross-linked points from the microcrystalline regions of PVA (Fig. 1d).

The physical crosslinks between PVA chains were elucidated by ATR-FTIR, as shown in Fig. 1f. The peaks at 2919, 1420 and 1090 cm^{-1} in the spectra of lyophilized gel are assigned to C-H stretching vibrations, C-H bending vibrations, and C-OH stretching vibrations, respectively [41, 42], which are characteristic peaks of PVA molecular. After the gel was lyophilized, the peak around 3355 cm^{-1} obviously shifted to the lower wavenumber of 3296 cm^{-1}, which probably indicated the formation of hydrogen bonding between hydroxyl groups of PVA chains [43]. In addition, the hydrogels prepared respectively by one and three freezing-thawing cycles are also tested by ATR-FTIR to detect hydrogen bonds indirectly. In Fig. S1, after three freezing-thawing cycles, the peak

of hydroxyl group is redshifted from 3364 cm^{-1} to 3355 cm^{-1}. These results confirm the hydrogen bonding crosslinking in PVA/H_2SO_4 hydrogel. Moreover, the crystal characteristic of PVA was detected by XRD spectra. The peak in the 2θ range 18° ~ 21° corresponds to $10\bar{1}$ crystal plane of PVA, suggesting the microcrystalline regions in PVA hydrogel. This result is consistent with the reports of the crystallinity of freezing-thawing PVA hydrogels of Rosa Ricciardi et al. [44, 45].

Figure 2

The self-healing procedure of PVA hydrogel is shown in Fig. 2. A piece of PVA hydrogel was cut into two halves, then the gel was healed successfully when the two halves were put contact and the fracture surfaces were overlapped. And even being lifted up, the healed specimen would not be broken again. In this test, the healing surface is formed by the fracture surfaces coming from the same specimen. To study the self-healing characteristics of fracture surfaces of different specimens, two pieces of hydrogels were cut in half, one of which was dyed red by rhodamine B to show the difference (Fig. 2b). Subsequently, the four cut pieces were brought into contact alternately and healed immediately. And even being lifted up and bent, the healed specimen assembled with different parts would not be broken again. These results show the outstanding self-healing performance of the PVA/H_2SO_4 hydrogel. On the one hand, the self-healing process can be realized at room temperature without any external stimulation (ultraviolet light, alternating current or pH value). On the other hand, even between two different fracture surfaces, there is still self-healing activity. Therefore, based on the above results, the self-

healing process can be illustrated in Fig. 2c. When the hydrogel is cut off, PVA networks in Fig. 1e will be damaged and the PVA chains will be cleavage and/or slippage. Then, the hydroxyl groups on the polyvinyl alcohol chains will be free, which endows the fracture surface with reactivity for healing. According to the self-healing model studied by Antonella Campanella et al. [46], on the fracture surface, hydroxyl groups which were originally in equilibrium state due to hydrogen bond breaking now become non-equilibrium state. After reassembling the cut pieces, the hydroxyl groups on different fracture surfaces will reassociate by diffusion of PVA chains to reform hydrogen bonds to re-establish the equilibrium state. For different fracture surfaces, there are also reactive hydroxyls on them, thus the self-healing behavior can still be effective.

Figure 3

The mechanical property plays a vital role in the application of flexible electrolyte. The PVA/H_2SO_4 hydrogel has been stretched uniaxially with a constant rate of 50 mm min^{-1}. Fig. 3a shows its stress-strain behavior, which exhibits a soft and tough elastic deformation in the tensile fracture curve. And the tensile strength can be 0.29 MPa, when elongation at break is 238 %. According to Rebeca Herna´ndez et al.'s study on viscoelastic properties of PVA hydrogel, the increased storage modulus of the gel obtained from multiple cycles may be due to the increase of molecular chains involved in hydrogen bonding [22]. Therefore, physical crosslinking including hydrogen bonding and microcrystalline achieved by freezing-thawing process provides the gel with outstanding mechanical properties. Then loading-unloading test has been carried out in order to

investigate the gel's energy dissipation ability (Fig. 3b). The hysteresis loops of the gel can be observed under various maximum extension ratios (λ_{max}), indicating that energy dissipation occurs inside the gel when it is stretched. And the energy dissipation of the gel shows a strain dependence that the hydrogel will exhibit greater energy dissipation at higher strain level. And the elastic modulus also becomes larger with the increasing of maximum extension ratios, which also be observed in the work of Xianqiang Yu et al. [17]. These results may be due to that the weak interactions such as hydrogen bonds will be broken primarily when the strain is small, then the entangled PVA chains will be rearranged and consume more energy as the strain increases. All these indicate good mechanical properties for the PVA/H_2SO_4 hydrogel prepared by freezing-thawing cycles.

Figure 4

The protons from sulfuric acid endow PVA/H_2SO_4 hydrogel with the ionic conductivity, which is measured by EIS and shown in Fig. 4a. Various H_2SO_4 concentration has been changed from 0.01 M to 3 M to be applied in PVA/H_2SO_4 hydrogel. And they do exhibit different ohmic resistance obtained from the intercept in the real axis., PVA/H_2SO_4 hydrogel electrolyte exhibits the largest ohmic resistance when the concentration of H_2SO_4 is as low as 0.01 M. On the contrary, the PVA/H_2SO_4 hydrogels with higher sulfuric acid concentration possess much lower ohmic resistance, indicating higher ionic conductivity. By the ohmic resistance from Fig 4a, the ionic conductivity of various PVA/H_2SO_4 hydrogels can be calculated and displayed in Fig. 4b. As the sulfuric acid concentration increases from 0.01 M to 1 M, the ionic conductivity increases rapidly

from 1.5 to 57.8 mS cm^{-1}. But when sulfuric acid concentration grows from 1M to 3 M, the ionic conductivity barely increases and eventually even decreases, which may because the sulfuric acid has been consumed by the reaction with the -OH on PVA. Thus, PVA/H_2SO_4 hydrogel with 1 M H_2SO_4 has been regarded as the most suitable gel electrolyte for supercapacitors.

Moreover, the self-healing property of PVA/H_2SO_4 hydrogel has been investigated by the ionic conductivity after several cut/healing cycles (Fig. 4 c and d) and the cut/healing process is shown in Fig. 2. With the increase of the cut/healing cycles, the intercept at the real axis gradually shifts to larger ohmic resistance in Fig. 4c. After once cut/healing cycle, the ionic conductivity of PVA/H_2SO_4 hydrogel is 37.9 mS cm^{-1} which has been restored about 71 %. Even after 10th healing, its ionic conductivity is still 25.9 mS cm^{-1} which is qualified as electrolyte. Before the 3rd healing, the self-healing property decays quickly. This may be because multiple repairs lead to a gradual decrease in the active groups on the fracture surface that can form hydrogen bonds with the hydroxyl group on the other side, resulting in the decline of self-healing performance. And in the first few cutting/healing cycles, the active group density was still large, so the loss rate was faster, and the self-healing performance decreased rapidly. The plots in Fig. 4e displays valid application of the ionic conductive PVA/H_2SO_4 hydrogel. A piece of hydrogel membrane could be applied as a conducting wire to connect a circuit with a LED bulb because of its ionic conductive property. When the hydrogel membrane was cut off, the bulb turned off immediately. And after the two halves of the gel have been put back together, the bulb

rekindled a red light which is slightly weaker than that when the gel was intact, demonstrating the gel's self-healing performance. Therefore, a self-healing supercapacitor can be assembled by integrated configuration based on this self-healing gel electrolyte.

Figure 5

In order to get outstanding capacitive performance, polyaniline (PANI) has been employed as electrode, which was in situ polymerized on the surface of PVA/H_2SO_4 hydrogel electrolyte as shown in Fig. 5a. Then a self-healing supercapacitor is assembled by cutting off the short-circuiting edge connection, forming an all-in-one configuration that a healable PVA/H_2SO_4 gel electrolyte layer was sandwiched by two PANI electrode layers. And the polymerization of aniline to PANI is shown in Fig. 5b where the reaction is initiated by APS and continued for 3 h at 0 ℃.

Fig. 5c shows a piece of PANI-PVA/H_2SO_4 supercapacitor which is coated by PANI on its top and bottom surface. The micromorphology of the surface of PANI-PVA/H_2SO_4 supercapacitor was shown in Fig. 5d. The stacked staggered short rods are the typical microstructure of PANI [38], indicating that PANI has firmly grown on the surface of PVA/H_2SO_4 gel membrane. After cutting off the edge connection, the cross section containing the PVA/H_2SO_4 electrolyte layer in middle is exposed in Fig. 5e. Detected by SEM, the middle part of the cross section displays a 3D network structure that belongs to the PVA/H_2SO_4 gel electrolyte. This absolutely different structure confirms the sandwiched PANI electrode-PVA/H_2SO_4 gel electrolyte-PANI electrode configuration.

To further investigate the electrode-electrolyte interface, SEM image and line-scanning of element nitrogen has been performed through the interface (Fig. 5g). The SEM image through the electrode-electrolyte interface shows a continuous morphology without clear demarcation, indicating the firmly integrating between PANI electrode layer and PVA/H_2SO_4 gel electrolyte layer. The nitrogen content was high on both sides and low in the middle from the line-scanning curve from energy dispersive spectrometer in Fig. 5h. Because nitrogen comes from PANI, the side layers contain more PANI than middle layer, which is consistent with the sandwiched configuration in Fig. 5e. By contrast, Carbon element is relatively homogeneous distributed through the cross section (Fig. S2), because both PVA and PANI contain it. Moreover, Nitrogen has also been detected in the middle layer though its content is low, which indicate that PANI or thumbnail PANI chains have embedded in the gel electrolyte.

Figure 6

The electrochemical performance of PANI-PVA/H_2SO_4 supercapacitors with various aniline concentration (0.05, 0.1, 0.2, 0.3 and 0.4 M) have been investigated by CV, GCD and EIS. In Fig. 6a, each CV curve exhibits remarkable redox peaks attributed to the pseudocapacitance characteristics of PANI. When aniline concentration is 0.2 M, the integrated area of CV curve reaches the largest, suggesting the best specific capacitance performance.

According to the formula $C_A = \frac{2 \times I \times t}{S \times V}$, the discharge time in the GCD curves (Fig. 6b) is affected by the specific area capacitance of various PANI-PVA/H_2SO_4 supercapacitors.

And discharge time also reaches the longest when aniline concentration is 0.2 M, resulting from the best capacitance performance. Then the specific area capacitance of various supercapacitors is shown in Fig. 6c. The specific capacitance increases rapidly with aniline concentration less than 0.2 M, but then goes down slowly. According to the research of Kai Wang et al. [15], the gelation of aniline solution will prevent the further increase of PANI loading amount when aniline concentration is high. Thus, in this work, the maximum specific area capacitance of 460 mF cm^{-2} was achieved with aniline concentration of 0.2 M.

Moreover, the electrochemical processes of these supercapacitors have been demonstrated by EIS, and are shown in the Nyquist plot in Fig. 6d. In low frequency area, the interpret of the curve at real axis shows the bulk resistance of whole device. The bulk resistance of 0.1 and 0.2 M aniline based device are similar (4.46 Ω and 4.63 Ω) and lower than that of others. In high frequency area, the straight line of the devices based on the 0.2 and 0.3 M aniline exhibit the larger slope, indicating the better capacitive property. Thus, the PANI (0.2)-PVA/H_2SO_4 supercapacitor, with the aniline concentration of 0.2 M, possess the best capacitive performance.

The electrochemical performance of the PANI (0.2)-PVA/H_2SO_4 supercapacitor has been demonstrated (Fig. 6e and f). The shape of CV curves at different scan rate is asymmetric and nonrectangular, as a result of the combination of electric double layer capacitor and pseudocapacitor, which is proved by non-isosceles triangle of GCD curves of the PANI (0.2)-PVA/H_2SO_4 supercapacitor at different current densities (Fig. 6f). In

addition, with elevated charge-discharge current, the supercapacitors display good rate capability (Fig. 6g). At the current density of 0.2 mA cm^{-2}, the PANI (0.2)-PVA/H_2SO_4 supercapacitor shows the largest specific area capacitance of 460 mF cm^{-2}. When the current density increases from 0.2 mA cm^{-2} to 3 mA cm^{-2} (15 times), the capacitance of the PANI (0.2)-PVA/H_2SO_4 supercapacitor keeps 77 %. Ying Guo et al. [16] has also researched PVA self-healing hydrogel electrolyte and prepared the all-in-one supercapacitor with SWCNT-PANI composite electrode, but the specific area capacitance was only 15.8 mF cm^{-2} at 0.044 mA cm^{-2} which is lower than this work. Fan Li et al. [47] had synthesized an all-solid-state supercapacitor based on polyaniline conducting polymer with the areal capacitance of 341.7 mF cm^{-2} at 0.25 mA cm^{-2}. Yueying Shen et al. [48] prepared the hybridized PANI/GO/CC nanofiber arrays electrode for an all-solid-state supercapacitor, and shown a specific capacitance of 335.4 mF cm^{-2} at 1 mA cm^{-2} which is a little lower than this work. Ragone plots in Fig. 6h show the energy density and power density of all supercapacitors. The PANI (0.2)-PVA/H_2SO_4 supercapacitor exhibits a large energy density of 32 μWh cm^{-2} while the power density is 100 μW cm^{-2}. And after the power density increased by 15 times, energy density is still 25 μWh cm^{-2}. Fig. 6i shows the cyclic stability of the PANI (0.2)-PVA/H_2SO_4 supercapacitor based on the GCD method at the current density of 2 mA cm^{-2}. With the increase of charge and discharge times, after 1000 cycles of charge and discharge, its capacitance retention rate remains about 81%, which proves its good electrochemical cycle stability.

Figure 7

Except the superior capacitive performance, the PANI-PVA/H_2SO_4 supercapacitor device also possesses self-healing property. In a self-healing process (Fig. 7a), a capacitor was broken into halves. And then they were connected by reassembling the fracture surface. Subsequently, the capacitor was healed integrally. This self-healing process can be illustrated by schematic Fig. 7b. After the device is broken, the PVA chains tethered on the fracture surface can move or rotate spontaneously, forcing the hydroxyl groups to re-form the hydrogen bond, thus repairing the device. In fact, PANI electrodes cannot achieve self-healing intrinsically, so the healing of the device is still dominated by PVA/H_2SO_4 electrolyte. Therefore, the PANI-PVA/H_2SO_4 membrane has been used as a conductor to connect a circuit with a LED bulb. After self-healing of PANI-PVA/H_2SO_4 membrane, the bulb rekindled with a slightly dimmed lighting indicating that the healed device remains electrical contact.

Figure 8

Additionally, the self-healing performance of the device has been researched by capacitance retention after several cut/healing cycles (Fig. 8). Fig. 8a shows the CV curves of the capacitor device under 0, 1, 3, 5 cut/healing cycles at scan rate of 5 mV s^{-1}. The current response is decreased as the increasing of cut/healing cycles, indicating the increasing device resistance, which may be due to the deteriorating electric contact of PANI electrode. The charge and discharge time are also becoming shorter with the increasing cut/healing cycles from the GCD curves at 5 mA cm^{-2} in Fig. 8b, indicating the decay of capacitive performance.

To investigate the electrochemical interfacial property, the device after several cut/healing cycles has been test ed by EIS and the Nyquist plots is shown in Fig. 8c. The bulk resistance represented by intercept at real axis also increases with the number of cut/healing cycles. The bulk resistance is converted to the conductivity and the healing ratio based on ionic conductivity of the device is obtained (Fig. 8d). The healing ratio based on the ionic conductivity of the electrolyte and the capacitance of device are also shown for comparison. The ionic conductivity of the device decays faster than that of pure electrolyte, indicating the gradual deterioration of electrical contact of the device. For ionic conductivity and capacitance of the device, capacitance decays faster but the difference between them is smaller.

These results suggest that the decrease of device capacitance is mainly due to the gradual deterioration of electrical contact at the fracture/healing surface. Furthermore, according to the view of Ying Yang et al [49], the stability of hydroxyl groups on PVA chains exposed on the fracture surface is the key factor affecting material healing and the self-healing process will compete with the environment around the hydroxyl group. On the one hand, these hydroxyl groups may lose reactivity as oxidation, water competition, or changes in molecular conformation when they are exposed in the air environment as the gel is damaged. On the other hand, from the line-scanning of nitrogen, thumbnail PANI chains have diffused into the gel electrolyte, which may also reduce the reactivity between the hydroxyl groups. Thus, the self-healing property of the gel electrolyte is diminished during the cut/healing cycles, which endow the all-in-one supercapacitor

device an incomplete electric contact and energy storage property.

4. Conclusions

In summary, by the all-in-one configuration as the assembly strategy and PVA hydrogel as the self-healing electrolyte, we constructed the all-in-one self-healing supercapacitor, which not only avoids the defects of the laminate design but also tightly combines the self-healing electrolyte with the electrode material. The PVA hydrogel electrolyte shows good mechanical properties (stress strength 0.29 MPa, strain 238%) and ionic conductivity (57.8 mS cm^{-1}), which satisfied the electrolyte application. It also shows excellent self-healing performance (after 10th healing, its ionic conductivity is still 48 %) which gradually decreased as the increase of the number of cut/healing cycles with the ionic conductivity as the scale, and the rate of decline gradually slowed down. In addition, after adjusting the concentration of aniline, supercapacitor also exhibits 470 mF cm^{-2} at current density of 0.2 mA cm^{-2} and a large energy density of 32 μWh cm^{-2} while the power density is 100 μW cm^{-2}. And it also possesses great self-healing performance (63% capacitance retention), which can be considered that the diffusion of thumbnail PANI chains in the gel electrolyte adversely affects the device's self-healing performance, after comparing with the self-healing performance of PVA. This work suggests a guideline for all-in-one self-healing supercapacitor design applied in wearable electronics.

Acknowledgements

This research was supported by "the Fundamental Research Funds for the Central Universities" (Grant 2019XKQYMS03). Fundamental Research Funds for the Central

Universities (CN)

Compliance with ethical standards

We declare that we do not have any commercial or associative interest that represents a conflict of interest in connection with the manuscript.

Reference

[1] M. Khatib, T.P. Huynh, Y. Deng, Y.D. Horev, W. Saliba, W. Wu, H. Haick, Small 15, 2 (2019)

[2] K. Li, Z. Xu, S. Zhao, X. Meng, R. Zhang, J. Li, J. Leng, G. Zhang, D. Cao, R. Sun, Chem. Eng. J. 371, 203(2019)

[3] J.H. Yoon, S.M. Kim, H.J. Park, Y.K. Kim, D.X. Oh, H.W. Cho, K.G. Lee, S.Y. Hwang, J. Park, B.G. Choi, Biosens. Bioelectron. 150, 111946 (2020)

[4] M. Liao, P. Wan, J. Wen, M. Gong, X. Wu, Y. Wang, R. Shi, L. Zhang, Adv. Funct. Mater. 27, 1703852 (2017)

[5] D.C. Wang, H.Y. Yu, D. Qi, M. Ramasamy, J. Yao, F. Tang, K.M.C. Tam, Q. Ni, ACS Appl. Mater. Interfaces 11, 24435 (2019)

[6] D. Son, J. Kang, O. Vardoulis, Y. Kim, N. Matsuhisa, J.Y. Oh, J.W. To, J. Mun, T. Katsumata, Y. Liu, A.F. McGuire, M. Krason, F. Molina-Lopez, J. Ham, U. Kraft, Y. Lee, Y. Yun, J.B. Tok, Z. Bao, Nat. Nanotechnol. 13, 1057(2018)

[7] M.S. Tsai, T.L. Shen, H.M. Wu, Y.M. Liao, Y.K. Liao, W.Y. Lee, H.C. Kuo, Y.C. Lai, Y.F. Chen, ACS Appl. Mater. Interfaces 12, 9755 (2020)

[8] J. Zhao, Y. Li, M. Wang, Mater. Res. Bull. 112, 292 (2019)

[9] Z. Wang, F. Tao, Q. Pan, J. Mater. Chem. A 4, 17732 (2016)

[10] R. Hu, J. Zhao, Y. Wang, Z. Li, J. Zheng, Chem. Eng. J. 360, 334 (2019)

[11] B. Zhang, J. Li, F. Liu, T. Wang, Y. Wang, R. Xuan, G. Zhang, R. Sun, C.P. Wong, Chem.-Eur. J. 25, 11715 (2019)

[12] K. Guo, N. Yu, Z. Hou, L. Hu, Y. Ma, H. Li, T. Zhai, J. Mater. Chem. A 5, 16(2017)

[13] J. Han, Q. Ding, C. Mei, Q. Wu, Y. Yue, X. Xu, Electrochim. Acta 318, 660 (2019)

[14] M. Chen, J. Chen, W. Zhou, J. Xu, C.-P. Wong, J. Mater. Chem. A 7, 26524 (2019)

[15] K. Wang, X. Zhang, C. Li, X. Sun, Q. Meng, Y. Ma, Z. Wei, Adv. Mater. 27, 7451 (2015)

[16] Y. Guo, K. Zheng, P. Wan, Small 14, 1704497 (2018)

[17] X. Yu, Y. Li, J. Yang, F. Chen, Z. Tang, L. Zhu, G. Qin, Y. Dai, Q. Chen,

Macromol. Mater. Eng. 303, 1800295 (2018)

[18] H. Liao, F. Zhou, Z. Zhang, J. Yang, Chem. Eng. J. 357, 428 (2019)

[19] J. Wang, F. Liu, F. Tao, Q. Pan, ACS Appl Mater Interfaces, 9, 27745(2017)

[20] D.L. Taylor, M. In Het Panhuis, Adv. Mater. 28, 9060 (2016)

[21] Y. Li, S. Chen, M. Wu, J. Sun, ACS Appl. Mater. Interfaces 6, 16409 (2014)

[22] R. Hernández, A. Sarafian, D. López, C. Mijangos, Polymer 45, 5543 (2004)

[23] K.K.H. Wong, J.L. Hutter, M. Zinke-Allmang, W. Wan, Eur. Polym. J.45, 1349 (2009)

[24] S. Das, U. Subuddhi, J. PHARM. ANAL. 9, 108(2019)

[25] A. Schulte, Q.F.M. Alhusaini, H. Schönherr, ACS Appl. Bio Mater. 3, 2419 (2020)

[26] S. Gupta, T.J. Webster, A. Sinha, J. Mater. Sci.-Mater. Med. 22, 1763 (2011)

[27] N. Samadi, M. Sabzi, M. Babaahmadi, Int. J. Biol. Macromol., 107, 2291 (2018)

[28] H. Peng, Y. Lv, G. Wei, J. Zhou, X. Gao, K. Sun, G. Ma, Z. Lei, J. Power Sources 431, 210 (2019)

[29] J. Han, H. Wang, Y. Yue, C. Mei, J. Chen, C. Huang, Q. Wu, X. Xu, Carbon 149, 1 (2019)

[30] H. Fei, C. Yang, H. Bao, G. Wang, J. Power Sources 266, 488 (2014)

[31] F. Tao, L. Qin, Z. Wang, Q. Pan, ACS Appl. Mater. Interfaces 9,15541 (2017)

[32] W. Zhao, L. Wei, Q. Fu, X. Guo, J. Power Sources 422, 73 (2019)

[33] Y.H. Liu, Z.Y. Jiang, J.L. Xu, ACS Appl. Mater. Interfaces 11, 24047 (2019)

[34] Y. Huang, M. Zhong, Y. Huang, M. Zhu, Z. Pei, Z. Wang, Q. Xue, X. Xie, C. Zhi, Nat. Commun. 6, 10310 (2015)

[35] Y. Bai, R. Liu, Y. Wang, H. Xiao, Y. Liu, G. Yuan, ACS Appl. Mater. Interfaces 11, 43294 (2019)

[36] J.P. Pouget, M.E. Jtizefowicz, A.J. Epstein, X. Tang, A.G. MacDiarmid, Macromolecules 24, 779 (1991)

[37] Y. Lin, H. Zhang, H. Liao, Y. Zhao, K. Li, Chem. Eng. J. 367, 139 (2019)

[38] J. Ma, X.-Y. Tao, S.-X. Zhou, X.-Z. Song, G. Lin, W. Yao, Y.-B. Zhu, L.-T. Guo, Z.-S. Liu, H.-L. Fan, X.-Y. Wei, J. Electroanal. Chem. 835, 346 (2019)

[39] S.-X. Zhou, X.-Y. Tao, J. Ma, L.-T. Guo, Y.-B. Zhu, H.-L. Fan, Z.-S. Liu, X.-Y. Wei, Vacuum 149, 175 (2018)

[40] S.-X. Zhou, X.-Y. Tao, J. Ma, C.-H. Qu, Y. Zhou, L.-T. Guo, P.-Z. Feng, Y.-B. Zhu, X.-Y. Wei, Vacuum 143, 63 (2017)

[41] S. Huang, S. Shuyi, H. Gan, W. Linjun, C. Lin, X. Danyuan, H. Zhou, X. Lin, Y. Qin, Carbohydr. Polym. 223, 115080 (2019)

[42] A. Olad, M. Eslamzadeh, A. Mirmohseni, J. Appl. Polym. Sci. 136, 48025 (2019)

[43] Y. Shi, Y. Zhang, L. Jia, Q. Zhang, X. Xu, ACS Appl. Mater. Interfaces 10, 36028 (2018)

[44] R. Ricciardi, F. Auriemma, C. Gaillet, C.D. Rosa, F.o. Laupreˆtre, Macromolecules 37, 9510 (2004)

[45] R. Ricciardi, F. Auriemma, C.D. Rosa, F.o. Laupreˆtre, Macromolecules 37, 1921 (2004)

[46] A. Campanella, D. Dohler, W.H. Binder, Macromol. Rapid Commun. 39, 17 (2018)

[47] F. Li, J. Liu, Y. Ma, Z. Shang, Q.-a. Huang, X. Huang, A monolithic integrated ultra-flexible all-solid-state supercapacitor based on a polyaniline conducting polymer, J. Mater. Chem. A 7, 15378 (2019)

[48] Y. Shen, Z. Qin, S. Hu, L. Yang, X. Xu, L. Ding, Y. Zhang, Carbon 158, 711 (2020)

[49] Y. Yang, M.W. Urban, Chem. Soc. Rev. 42, 7446 (2013)

Captions to the figures:

Fig. 1 (a-d) Schematic of preparation process of physical crosslinking PVA/H_2SO_4 hydrogel electrolyte membrane. (e) The progress that PVA chains are crosslinked by hydrogen bond. (f) ATR-FTIR spectra of PVA hydrogel and lyophilized gel. (g) XRD spectra of the lyophilized gel.

Fig. 2 (a) Self-healing process of PVA/H_2SO_4 hydrogel. (b) The self-healing between different fracture surface. (d) Schematic of mechanism of the self-healing process.

Fig. 3 (a) Stretch stress-strain curve, (b) loading-unloading test under various maximum extension ratios and (c) Picture of stretch progress of PVA/H_2SO_4 hydrogel electrolyte.

Fig. 4 (a) EIS and (b) Ionic conductivity vs the different concentrations of H_2SO_4: 0.01M, 0.5M, 1M and 2M for PVA/H_2SO_4 hydrogel electrolyte. (c) High frequency area of EIS and (d) Ionic conductivity of 1M H_2SO_4 PVA hydrogel electrolyte after several cutting/healing cycles.

Fig. 5 (a) Schematic diagram of the preparation of all-in-one PANI-PVA/H_2SO_4 supercapacitor. (b) The polymerization of aniline. (c) An optical image of PANI-PVA/H_2SO_4 supercapacitor and (d) SEM image of its surface layer. (e) Optical image of the cross section of PANI-PVA/H_2SO_4 supercapacitor and (f) SEM of the middle layer. (g) The SEM image of the cross section of PANI-PVA/H_2SO_4 membrane and the path of Nitrogen line-scanning over it. (h) The distribution of line-scanning of Nitrogen.

Fig.6 (a) CV at different scan rates of 5 mV s^{-1}, (b) GCD (discharge curves) at current densities of 0.2 mA cm^{-2}, (c) specific area capacitance and (d) Nyquist plots of all-in-one PANI-PVA/H_2SO_4 supercapacitors different with different aniline concentration. (e) CV and (f) GCD curves of the PANI(0.2)-PVA/H_2SO_4 supercapacitor. (g) Rate capability and (h) Ragone plots of all-in-one PANI-PVA/H_2SO_4 supercapacitors with different aniline concentration. (i) The capacitance retention of PANI(0.2)-PVA/H2SO4 supercapacitor

Fig. 7 (a) The self-healing process of the all-in-one PANI-PVA/H_2SO_4 supercapacitor. (b) Schematic illustration of the mechanism of the self-healing process in (a). (c) PANI-PVA/H_2SO_4 membrane is served as a conductor in a circuit with a LED bulb.

Fig. 8 (a) CV curves, (b) GCD curves and (c) Nyquist plots of the PANI (0.2)-PVA/H_2SO_4 supercapacitor device under 1, 3, 5 cut/healing cycles. (d) Capacitance and ionic conductivity healing ratio of the device under 1, 3, 5 cut/healing cycles.

Figures

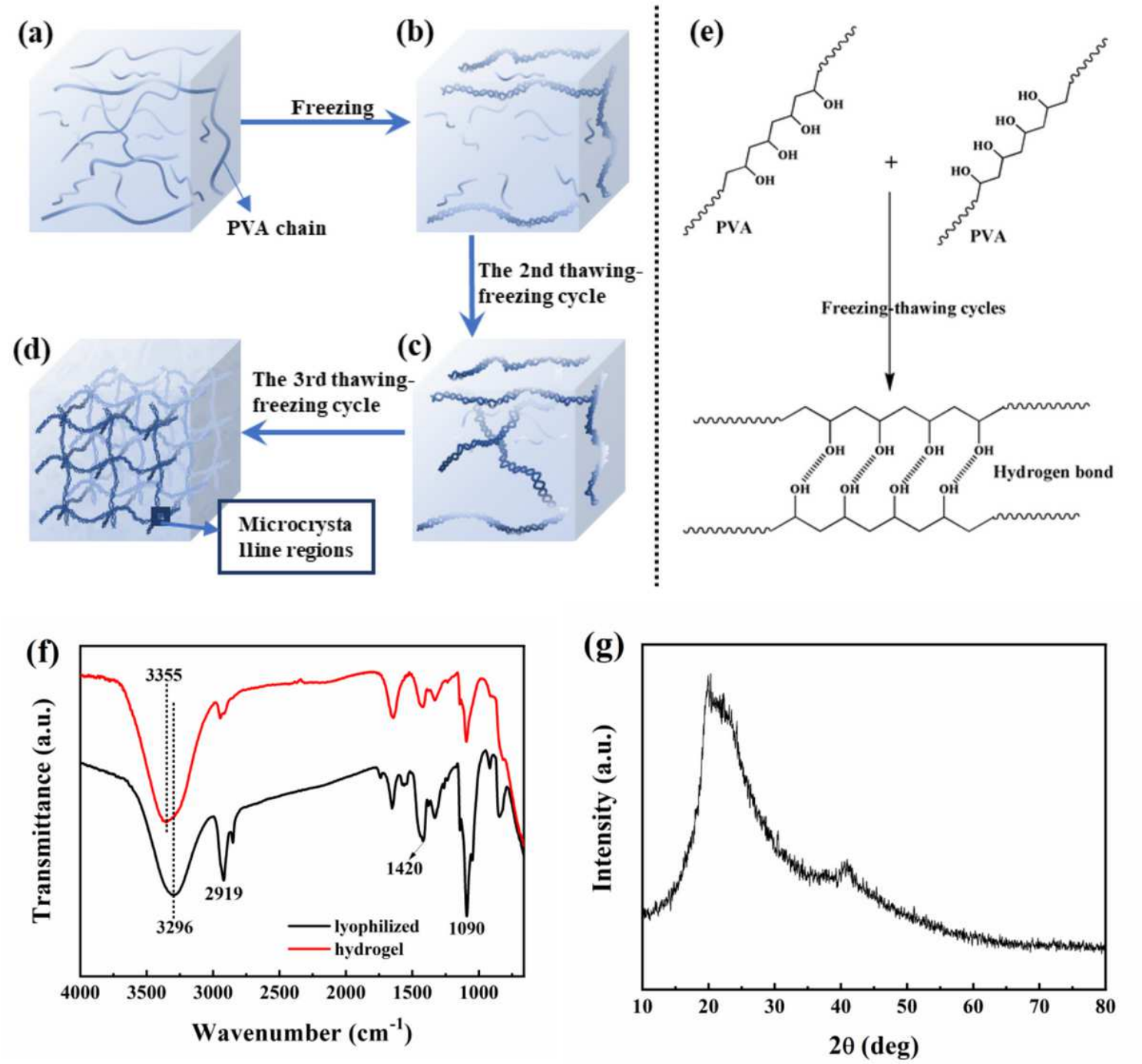

Figure 1

(a-d) Schematic of preparation process of physical crosslinking PVA/H2SO4 hydrogel electrolyte membrane. (e) The progress that PVA chains are crosslinked by hydrogen bond. (f) ATR-FTIR spectra of PVA hydrogel and lyophilized gel. (g) XRD spectra of the lyophilized gel.

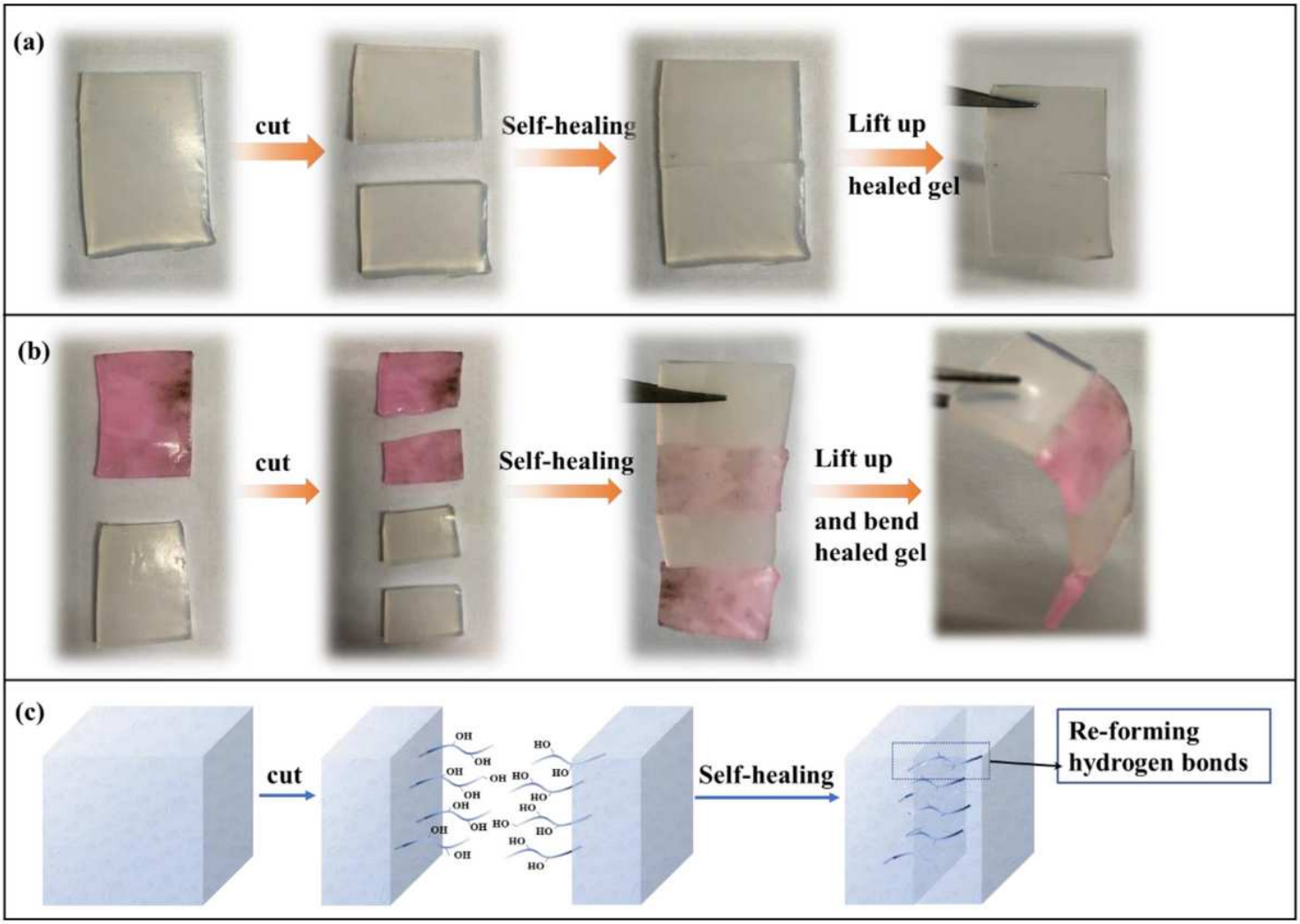

Figure 2

(a) Self-healing process of PVA/H2SO4 hydrogel. (b) The self-healing between different fracture surface. (d) Schematic of mechanism of the self-healing process.

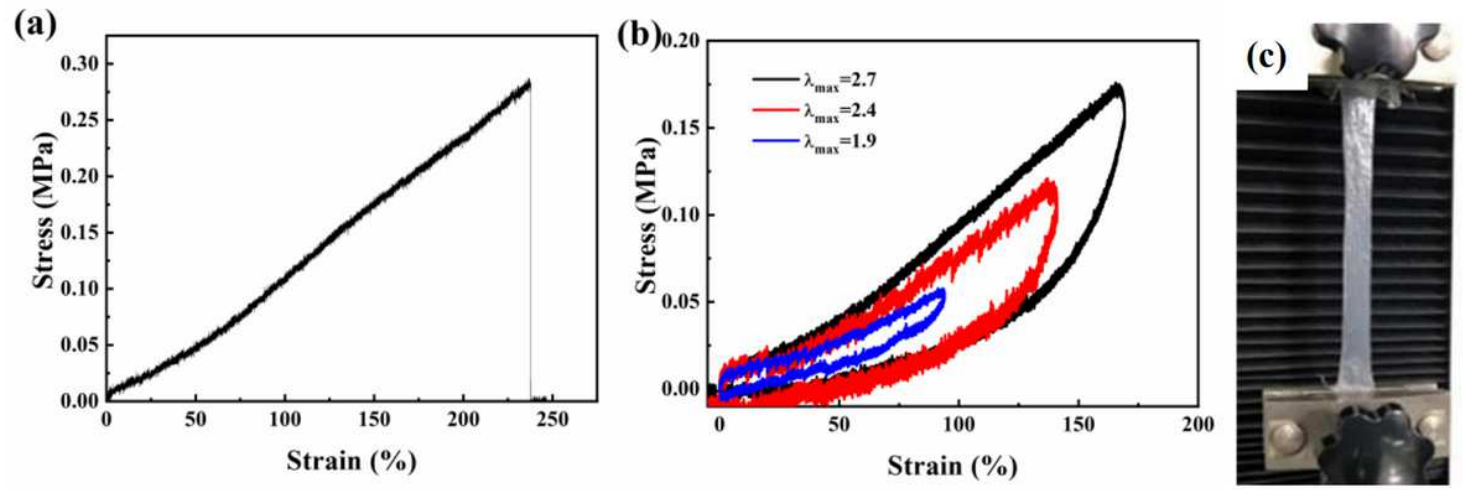

Figure 3

(a) Stretch stress-strain curve, (b) loading-unloading test under various maximum extension ratios and (c) Picture of stretch progress of PVA/H2SO4 hydrogel electrolyte.

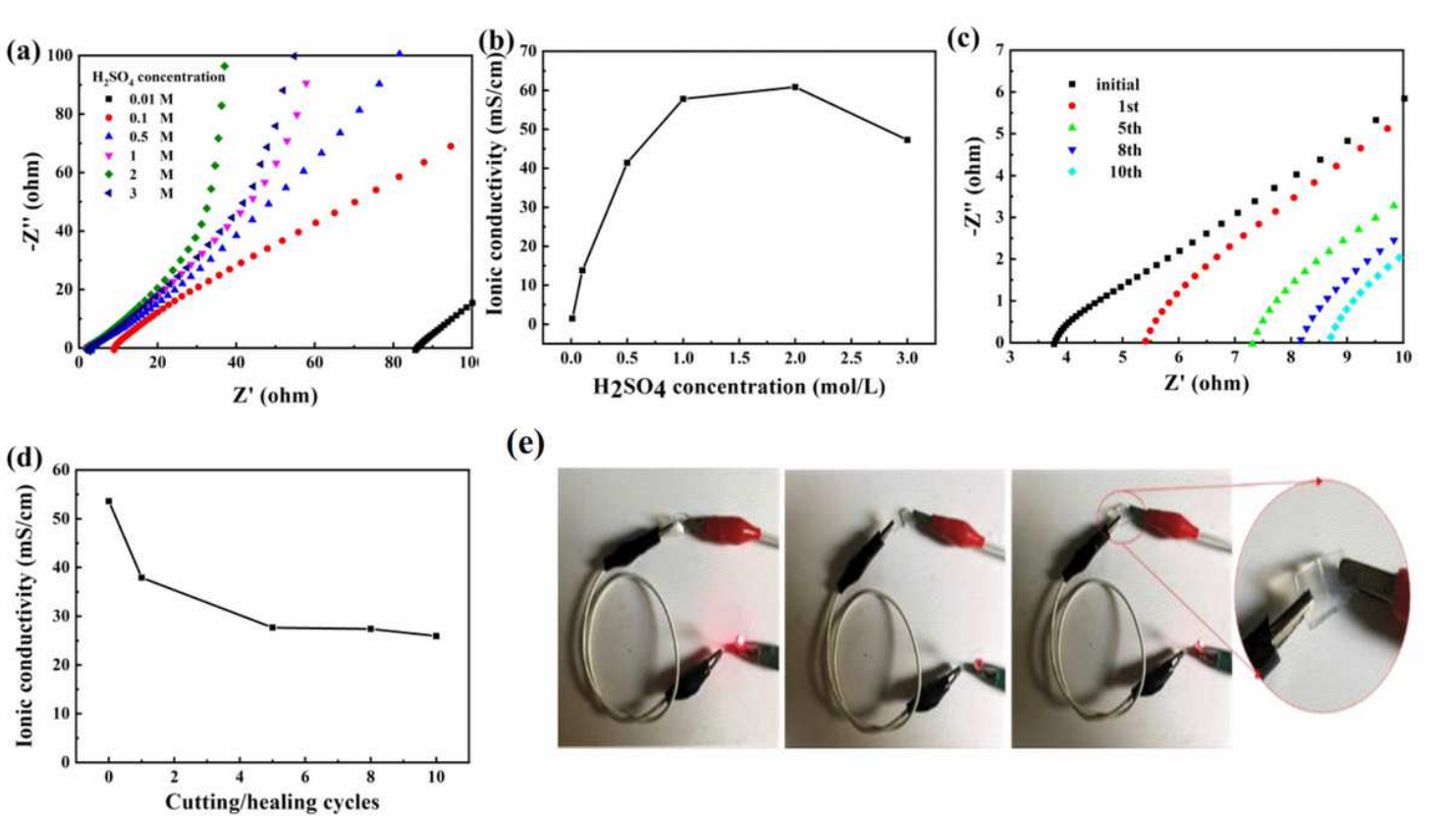

Figure 4

(a) EIS and (b) Ionic conductivity vs the different concentrations of H2SO4: 0.01M, 0.5M, 1M and 2M for PVA/H2SO4 hydrogel electrolyte. (c) High frequency area of EIS and (d) Ionic conductivity of 1M H2SO4 PVA hydrogel electrolyte after several cutting/healing cycles.

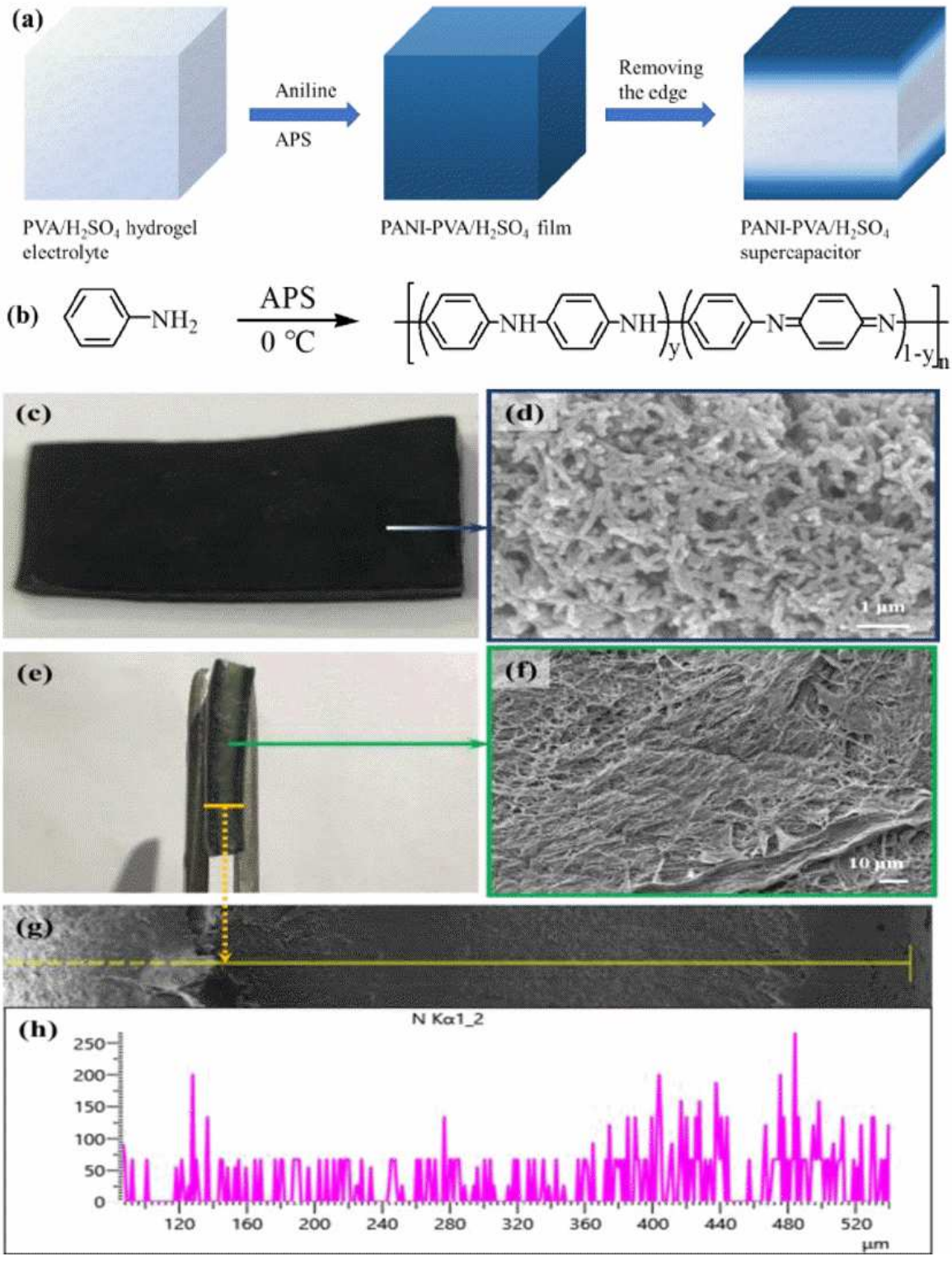

Figure 5

(a) Schematic diagram of the preparation of all-in-one PANI-PVA/H2SO4 supercapacitor. (b) The polymerization of aniline. (c) An optical image of PANI-PVA/H2SO4 supercapacitor and (d) SEM image of its surface layer. (e) Optical image of the cross section of PANI-PVA/H2SO4 supercapacitor and (f) SEM of the middle layer. (g) The SEM image of the cross section of PANI-PVA/H2SO4 membrane and the path of Nitrogen line-scanning over it. (h) The distribution of line-scanning of Nitrogen.

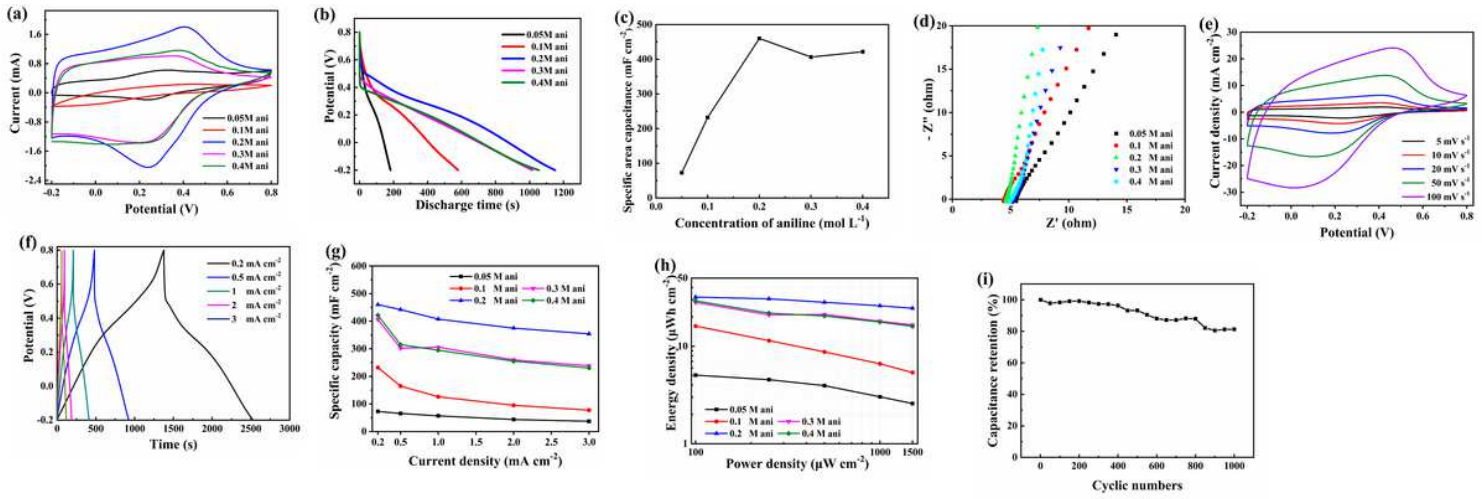

Figure 6

(a) CV at different scan rates of 5 mV s−1, (b) GCD (discharge curves) at current densities of 0.2 mA cm-2, (c) specific area capacitance and (d) Nyquist plots of all-in-one PANI-PVA/H2SO4 supercapacitors different with different aniline concentration. (e) CV and (f) GCD curves of the PANI(0.2)-PVA/H2SO4 supercapacitor. (g) Rate capability and (h) Ragone plots of all-in-one PANI-PVA/H2SO4 supercapacitors with different aniline concentration. (i) The capacitance retention of PANI(0.2)-PVA/H2SO4 supercapacitor

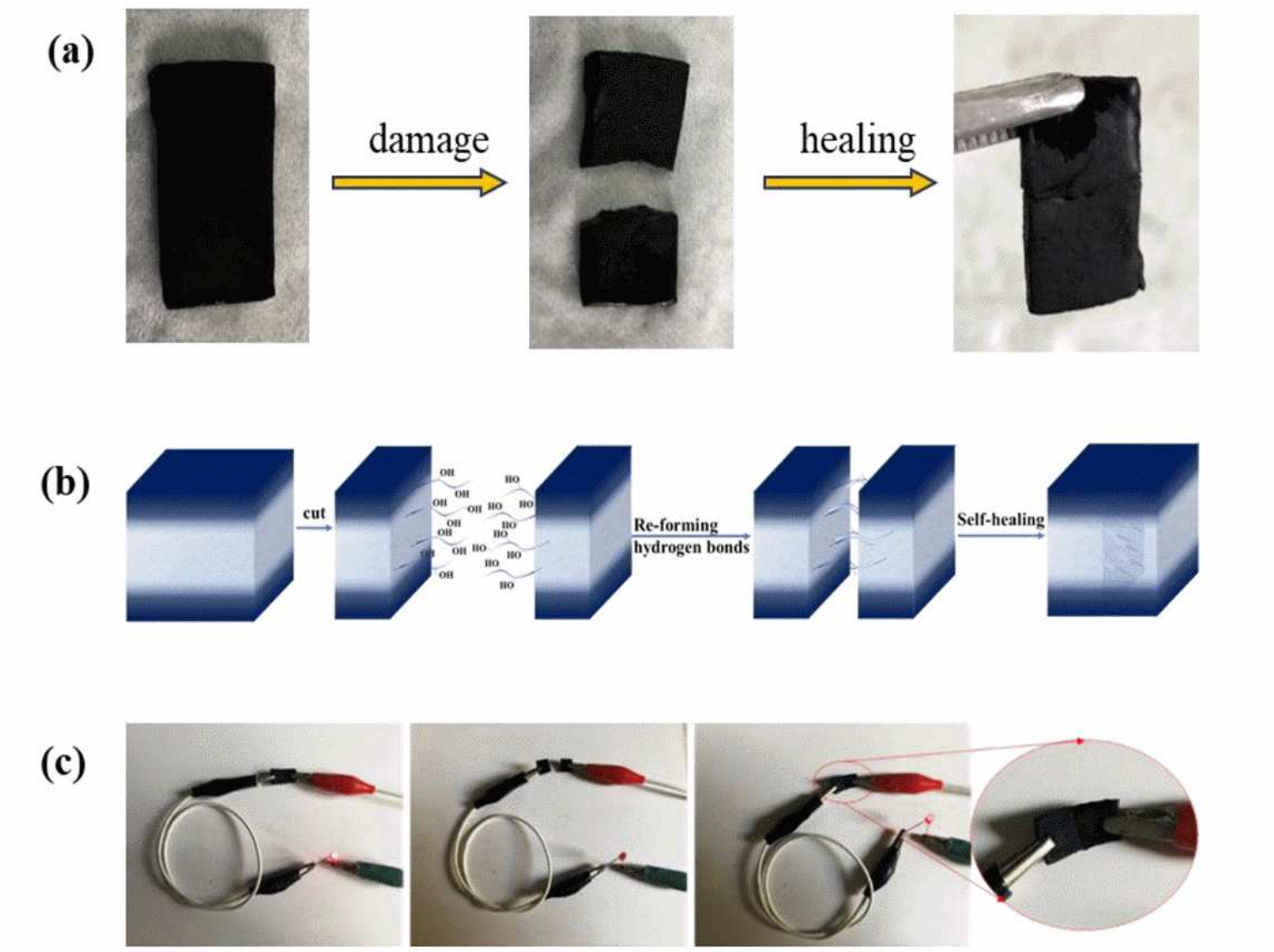

Figure 7

(a) The self-healing process of the all-in-one PANI-PVA/H2SO4 supercapacitor. (b) Schematic illustration of the mechanism of the self-healing process in (a). (c) PANI-PVA/H2SO4 membrane is served as a conductor in a circuit with a LED bulb.

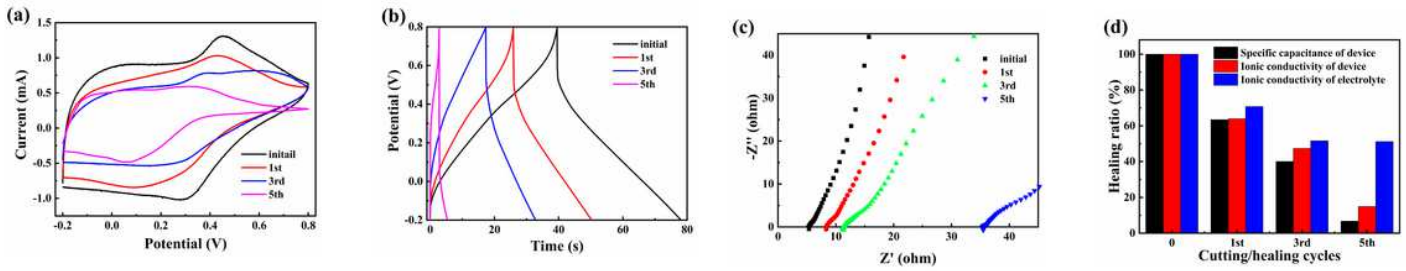

Figure 8

(a) CV curves, (b) GCD curves and (c) Nyquist plots of the PANI (0.2)-PVA/H2SO4 supercapacitor device under 1, 3, 5 cut/healing cycles. (d) Capacitance and ionic conductivity healing ratio of the device under 1, 3, 5 cut/healing cycles.

Supplementary Files

This is a list of supplementary files associated with this preprint. Click to download.

- SupplementaryInformation.pdf